THE JOURNAL OF PHYSICAL CHEMISTRY Letters

Letter

Cite This: J. Phys. Chem. Lett. 2019, 10, 3094−3100

pubs.acs.org/JPCL

Realization of the Photostable Intrinsic Core Emission from Carbon Dots through Surface Deoxidation by Ultraviolet Irradiation

Minghong Sun,[†,‡,⊥] Chao Liang,[¶,⊥] Zhen Tian,[†,‡,⊥] Elena V. Ushakova,[§,⊥] Di Li,[†] Guichuan Xing,[¶] Songnan Qu,[*,¶] and Andrey L. Rogach[§,∥]

[†]State Key Laboratory of Luminescence and Applications, Changchun Institute of Optics, Fine Mechanics and Physics, Chinese Academy of Sciences, Changchun 130033, China

[‡]University of Chinese Academy of Sciences, Beijing 100049, China

[¶]Joint Key Laboratory of the Ministry of Education, Institute of Applied Physics and Materials Engineering, University of Macau, Taipa, Macau, China

[§]Center of Information Optical Technologies, ITMO University, Saint Petersburg 197101, Russia

[∥]Department of Materials Science and Engineering, City University of Hong Kong, 83 Tat Chee Avenue, Kowloon, Hong Kong, China

Supporting Information

ABSTRACT: It is of a primary importance to realize the intrinsic emission from the inner carbogenic cores of carbon dots (CDs). In this work, CDs with three emission centers were synthesized by a microwave-assisted method using phloroglucinol as a precursor. The emission of these three centers has been identified as originating from molecular fluorophores, surface states of CDs, and the intrinsic CD core state. The emission from molecular fluorophores and from the surface state of CDs exhibited a weak photostability and could be photobleached as a result of UV laser irradiation. The emission from the intrinsic state of the inner carbogenic core has been found to be stable against photobleaching. On the basis of this difference in photostability, we demonstrate how the surface of CDs can be deoxidized under prolonged UV irradiation, resulting in a narrow intrinsic emission with a photoluminescence quantum yield of 17%.

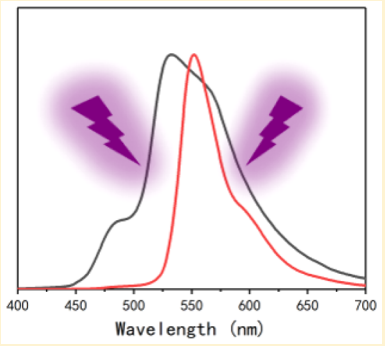

Luminescent carbon dots (CDs) are of considerable interest because of their ease of fabrication, nontoxicity,[1−3] and strong photoluminescence (PL).[4−7] Bottom-up approaches are widely used for the CD synthesis and occur via dehydration and carbonization processes of organic molecules/polymers containing carboxyl,[8−10] hydroxyl,[11] amides,[12−15] or amino[5,16−18] groups under solvothermal or microwave heating conditions.[19] This often results in the concurrent formation of molecular fluorophores or energy traps at the surface of carbongenic cores, which gives rise to the coexistence of the molecular fluorophore-related,[20,21] surface state,[22] and intrinsic state[23] emissions of the resulting samples. Thus, the PL origin is difficult to ascertain because CD emission possesses variable channels of radiative energy dissipation, typically resulting in excitation-dependent and broadened emission band. Several studies devoted to the photostability of CDs under UV irradiation[24−28] have shown that the emission from the confined sp^2 domains in carbogenic core (intrinsic state) are more stable than that from the surface states and molecular fluorophores, which are also typically located at the CD surface. It is of primary importance to be able to produce CDs with predominantly intrinsic emission with a narrow PL band, which can be done by fabrication of well-carbonized inner cores and by altering all other possibly existing channels of photoexcitation energy relaxation to enhance a purely intrinsic luminescence of CDs.

Recently, Yuan et al.[29] reported CDs produced by a solvothermal method using phloroglucinol as the precursor, with extremely narrow PL bands with a full width at half-maximum (fwhm) under 30 nm, which were ascribed to carbogenic cores. These CDs were successfully applied in light-emitting devices, and their electroluminescence spectra showed high color purity as well, with fwhm under 40 nm. This work provided a good base to follow up on such CD systems in order to further investigate and modulate their intrinsic core emission.

Herein, CDs were synthesized by a microwave-assisted method using phloroglucinol (PG) as precursor, and on the basis of the steady-state PL and transient absorption (TA) spectra, three luminescent centers (at 484, 528, and 550 nm) were revealed for these samples, which were assigned to the surface-located molecular fluorophores, CD surface states, and CD intrinsic core state, respectively. Spectral positions of any of these PL bands as such were found to be excitation-

Received: March 25, 2019
Accepted: May 21, 2019
Published: May 22, 2019

DOI: 10.1021/acs.jpclett.9b00842
J. Phys. Chem. Lett. 2019, 10, 3094−3100

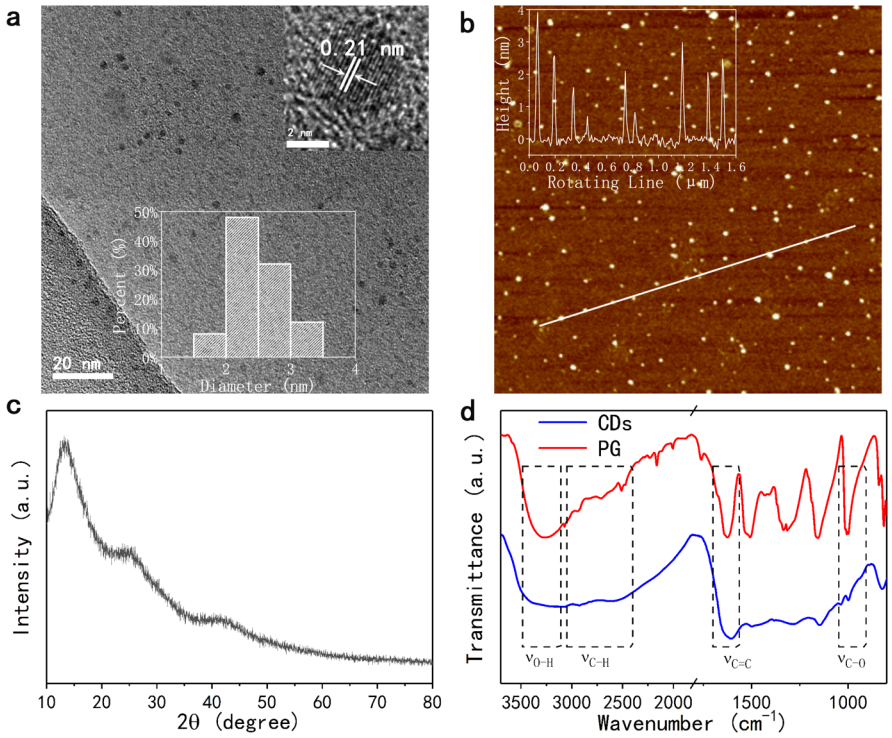

Figure 1. (a) TEM and HRTEM (inset) images and (b) AFM image of CDs. The size histogram and the height distribution profile are superimposed on the images. (c) XRD and (d) FT-IR spectra of CDs and their precursor PG.

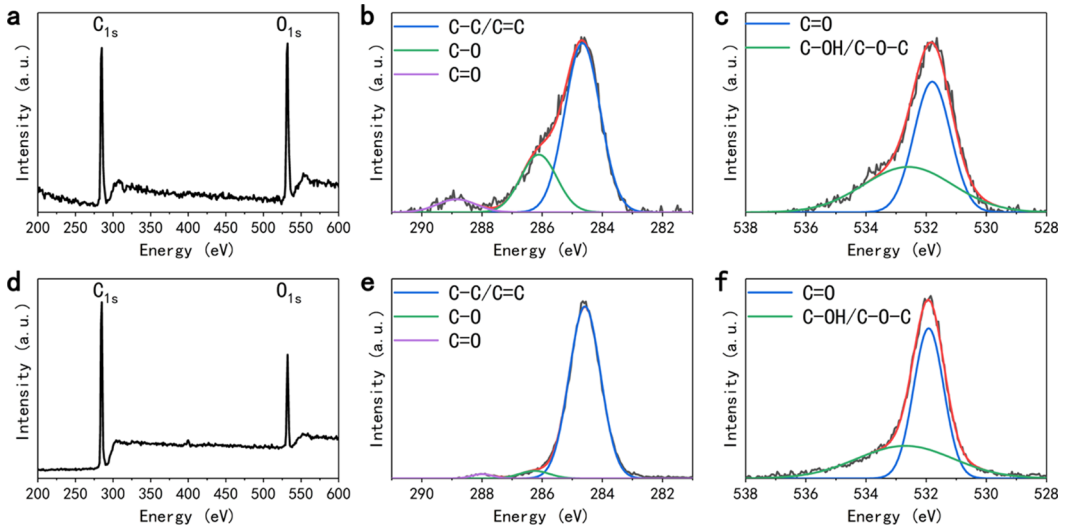

Figure 2. Full range XPS spectra of (a) CDs and (d) CDs-i, C_{1s} spectra of (b) CDs and (e) CDs-i, and O_{1s} spectra of (c) CDs and (f) CDs-i.

independent, while the overall emission profile of CDs was excitation-dependent because of the varying contribution of the three components. Under prolonged UV laser irradiation, the emissions from the molecular fluorophores and the surface state of CDs have been photobleached, while the emission from the intrinsic state of the inner carbogenic core with a narrow fwhm of 38 nm was enhanced, which has been ascribed to the surface deoxidation of CDs under UV irradiation. To the best of our knowledge, this is the first realization of the intrinsic emission from CDs through the surface deoxidation by UV irradiation.

The morphology of CDs was characterized by transmission electron microscopy (TEM) and atomic force microscopy (AFM). The TEM image provided in Figure 1a shows that CDs are spherical nanoparticles with diameters of 2−4 nm. The high-resolution TEM (HRTEM) image of a single CD (inset in Figure 1a) exhibits well-resolved lattice fringes with a spacing of 0.21 nm, which is consistent with the (100) crystal plane of graphitic carbon.[6] From the AFM profile (Figure 1b), the height of CDs has also been estimated as 2−4 nm, in good agreement with TEM data. Figure 1c shows the X-ray diffraction spectrum (XRD) of the CD powder, which exhibits the main diffraction peak at 13.2° and two less intense, wider peaks at 26.2° and 42.4°. In general, the diffraction peak of the (001) lattice plane in graphite cannot be observed in the XRD pattern, but it can be observed in the graphite oxide through the appearance of the peak around 13°, which is often used to identify graphite oxide structures.[30,31] The peak at 42.4° is

DOI: 10.1021/acs.jpclett.9b00842
J. Phys. Chem. Lett. 2019, 10, 3094−3100

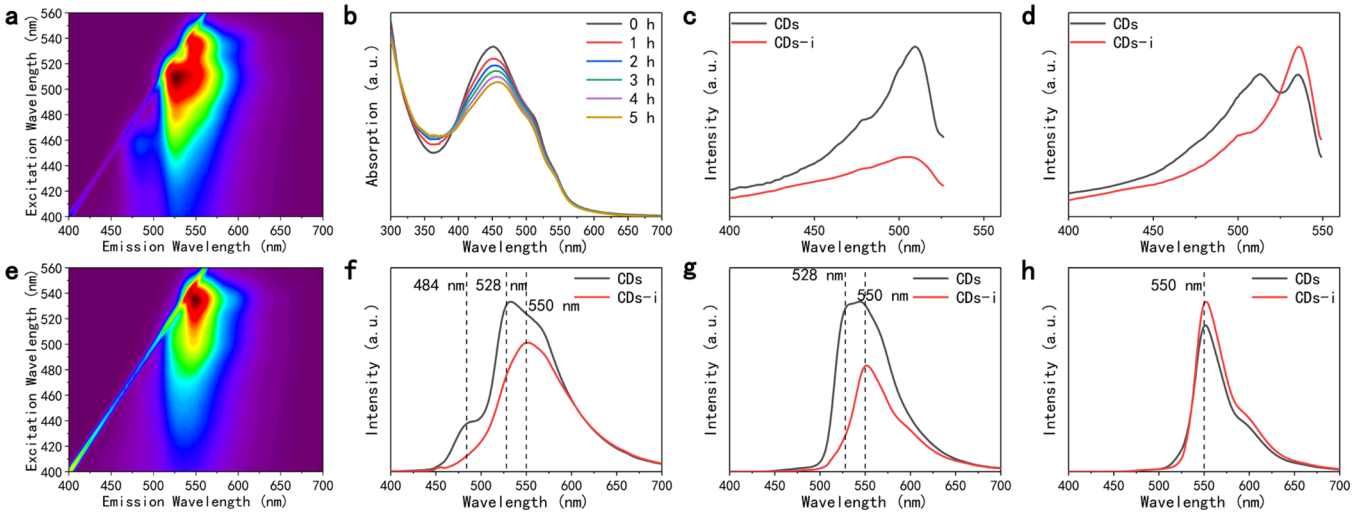

Figure 3. PL excitation−emission maps of (a) CDs and (e) CDs-i. (b) UV−vis absorption spectra of CDs before and after UV laser irradiation for different times (360 nm, 5730 W/m^2). PLE spectra of CDs and CDs-i monitored at (c) 528 nm and (d) 550 nm. PL spectra of CDs and CDs-i excited at (f) 450 nm, (g) 520 nm, and (h) 532 nm.

related to the (100) lattice plane of graphite, in accord with HRTEM observation. Considering the small size of CDs, the two peaks at 13.2° and 26.2° most likely originate from their graphite core with a highly oxidized surface.[32,33]

The chemical composition of CDs was investigated by Fourier transform infrared (FT-IR), X-ray photoelectron spectroscopy (XPS), and energy dispersive X-ray spectrometry (EDX). When FT-IR spectra of PG and CDs (Figure 1d) are compared, it can be seen that the relative intensity of the stretching vibration of O−H (ν_{O-H}) at about 3276 cm^{-1} and the stretching vibration of C−O (ν_{C-O}) at about 1007 cm^{-1} in CDs decreases, while the relative intensity of the stretching vibration of C−H in the aromatic ring (ν_{C-O}) at 3079 and 2615 cm^{-1} and aromatic ring skeleton vibration (ν_{C-O}) at 1607 cm^{-1} increases in CDs. Thus, it can be concluded that PG molecules are dehydrated and carbonized to form CDs with a graphitic core. In Figure 2a, the XPS spectrum of CDs exhibits two peaks at 284.0 and 531.5 eV, which are attributed to C_{1s} and O_{1s}, respectively,[2] indicating that CDs are composed of C and O elements. The C_{1s} spectrum (Figure 2b) contains three peaks at 288.9, 286.1, and 284.5 eV, which are attributed to O=C−O, C−O, and C−C/C=C groups, respectively. The O_{1s} spectrum (Figure 2c) contains two peaks at 531.8 and 532.6 eV, which are attributed to C=O and C−OH/C−O−C groups.[9] These data show that the surface of CDs contains abundant hydroxyl (−OH), ester (−OOCH), and epoxy (−C−O-C−) groups. It can be inferred that these groups are localized around the graphitic cores because of the highly oxidized surface.

The morphology and chemical structural changes of CDs after 5 h of UV irradiation (360 nm, 5730 W/m^2) were further investigated. The resulting CD sample is designated hereafter as CDs-i. Figures S1 and S2 show the TEM and AFM images of CDs-i. There was no obvious change in morphology of CDs and CDs-i. However, the chemical composition of the surface has changed; in particular, the content of oxygen was significantly reduced in CDs-i, which was revealed by EDX and XPS data, as shown in Figure S3 and 2a,d. EDX elemental analysis shows that the content of oxygen element is decreased from 25.9% to 13.1% in CDs and CDs-i, respectively, which agree well with the XPS results. In addition, from the C_{1s} spectra, it can be seen that the content of C−O in CDs-i greatly decreased from 24.3% to 3.9% (Figure 2b and e), indicating that the surface of CDs has been deoxidized after UV irradiation. We speculate that UV light-induced charge separation could happen in the CDs, making the surrounding solvent molecules ionized and generate solvated electrons,[34] which can be a deoxidizer, leading to the decreased oxygen content of CDs-i. Similar UV laser-induced deoxidation was reported for graphene oxide (GO) structures: Cao et al.[35] showed that UV irradiation can reduce GO into rGO, and Wang et al.[36] used UV irradiation to reduce GO in GO/TiO_2 nanoparticle hybrid films. Thus, it can be inferred that UV irradiation is able to reduce the surface oxygen content in CDs.

The absorption spectrum of the CDs in a diluted ethanol solution is shown in Figure 3b. CDs exhibit broad absorption in the 400−600 nm region, with the strongest absorption band centered at 450 nm and two shoulders at 510 and 534 nm. The PL excitation−emission map of CDs is provided in Figure 3a. There are three luminescent centers located at 484, 528, and 550 nm, with the most efficient excitation wavelengths located at 460, 512, and 532 nm, respectively. The PL spectra of CDs under 450, 520, and 532 nm laser excitations are shown in panels f, g and g of Figure 3, respectively. Under 450 nm excitation, there are three obvious emission bands peaked at 484, 528, and 550 nm, with an overall fwhm of 100 nm. Under 520 nm excitation, two emission bands peaked at 528 and 550 nm are observed, with an overall fwhm of 65 nm. In contrast, only one sharp emission band at 550 nm with a fwhm of 39 nm is observed under 532 nm excitation. The PL bands of three emission centers (484, 528, and 550 nm) are excitation-independent, while the total emission spectrum and its fwhm exhibit obvious excitation dependence. This indicates the varied contributions of the three emission centers to the total PL signal under different excitation wavelengths.

Absorption, PLE, and PL spectra of CDs-i are also presented in Figure 3. As shown in Figure 3b, the intensity of their major absorption bands gradually decreased and red-shifted, accompanied by gradually increased absorption intensity around 370 nm upon UV irradiation from 0 to 5 h. These changes can be due to photobleaching of the molecular fluorophores and deoxidization of the surface by the UV

DOI: 10.1021/acs.jpclett.9b00842
J. Phys. Chem. Lett. 2019, 10, 3094−3100

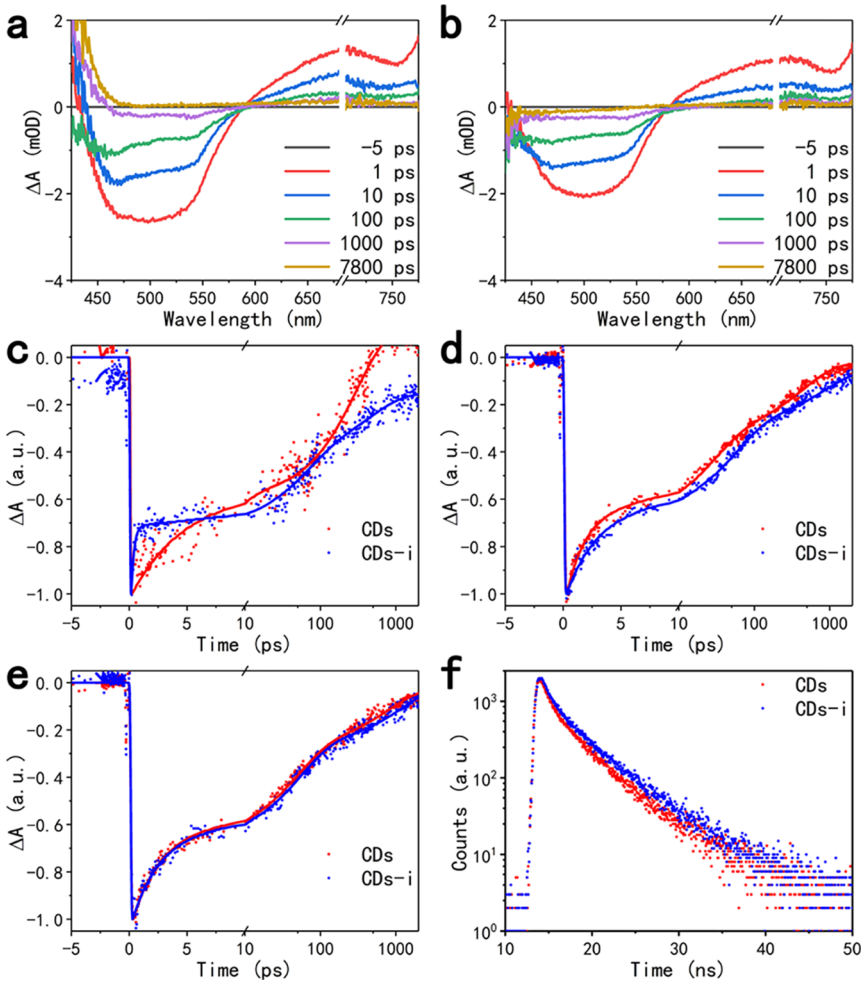

Figure 4. TA spectra at different delay times for (a) CDs and (b) CDs-i. TA kinetic traces of CDs and CDs-i collected at (c) 460 nm, (d) 512 nm, and (e) 532 nm following excitation at 350 nm with 100 fs, 1 kHz, and 2 μJ/cm^2 laser pulses. (f) Fluorescence decay curves of the CDs and CDs-i monitored at 550 nm.

irradiation. Comparing the PL excitation−emission maps of CDs and CDs-i (Figure 3a versus 3e), it can be seen that the PL signal from the two emission centers at 484 and 528 nm in CDs became almost quenched, while the emission band at 550 nm became dominant in CDs-i. The PL quantum yield (QY) increased from 13% for CDs to 17% for CDs-i (measured with excitation at 532 nm). Furthermore, after 5 h of UV irradiation, the fwhm of PL bands measured under 450, 520, and 532 nm excitations decreased to 87, 52, and 38 nm, respectively, as shown in Figure 3f−h. Considering the intrinsic state of the CDs as more photostable than the surface states and the molecular fluorophores, it is logical to assume that the emission center at 550 nm originates from the intrinsic state of the carbogenic core, while the other two emission centers (at 484 and 528 nm) belong to the molecular fluorophores and to the surface states of CDs, respectively.

The PL excitation (PLE) spectra of CDs and CDs-i in diluted ethanol solutions monitored at their 528 and 550 nm emission peaks are shown in Figure 3c,d. For CDs, there are two PLE bands peaked at 475 and 512 nm when monitored at 528 nm emission and two PLE bands peaked at 512 and 532 nm with a shoulder band around 450−480 nm when monitored at 550 nm emission. For CDs-i, the PLE bands at 475 and 512 nm greatly decreased, while the PLE band at 532 nm has been enhanced. These results indicate that the energy transfer may occur in CDs from the 460 nm energy band to the 512 nm energy band, giving rise to the 528 nm emission band, and from the 460 and 512 nm energy bands to the 532 nm energy band, giving rise to the 550 nm emission band. These energy-transfer processes are greatly diminished in CDs-i, which is due to the UV irradiation-induced deterioration of the 460 and 512 nm energy bands.

To further investigate the origin and carrier kinetics of the three emission centers in CD samples, femtosecond transient absorption (TA) measurements were conducted on the CDs and CDs-i in diluted ethanol solutions (Figure 4). The samples were first pumped with 350 nm (100 fs, 1 kHz, 2 μJ/cm^2) laser pulses, and photoinduced changes in absorption (ΔA) were probed with a time-delayed laser-generated white light probe pulses. The state filling originated from electrons in the ground state pumped into excited states, resulting in the ground-state bleaching feature, which is located from 450 to 600 nm in the TA spectra (Figure 4a,b). This broad photobleaching band is consistent with the broad band photon absorption in CDs in the same wavelength range (see Figure 3b). By comparing the TA spectra, it can be seen that the relative ground-state bleaching signals of CDs-i became reduced at the initial time upon photoexcitation, particular in the wavelength range from 430 to 520 nm, which is in agreement with their steady-state absorption spectra (Figure 3b). There were no additional

DOI: 10.1021/acs.jpclett.9b00842
J. Phys. Chem. Lett. 2019, 10, 3094−3100

photobleaching peaks emerged for CDs-i. These results indicate that the part of the transitions associated with bands in the range of 430−520 nm was eliminated upon UV irradiation, while the band around 532 nm (intrinsic state of CD core) possessed much better photostability. The TA kinetic traces at 460, 512, and 532 nm for the CDs and CDs-i are shown in panels c, d, and e of Figure 4, respectively. The changes in optical density can be well fitted by the three-exponential functions, and the evaluated decay parameters are listed in Table S1. It can be seen that photobleaching at 460 nm for CDs-i has a faster decay followed by a prolonged decay, which indicates that the absorption band at 460 nm is not only unstable but also sensitive to new species generated by UV irradiation. In contrast, the photobleaching decays at 512 and 532 nm for CDs-i became slightly prolonged. The fluorescence decays of CDs and CDs-i at 484, 528, and 550 nm were also measured at 405 nm ps laser excitation, as shown in Figures S6 and 4f. The fitting parameters of the PL decay curves are listed in Table S1. It can be seen that the PL lifetimes of CDs-i are all prolonged in comparison with those of the initial CDs.

Considering the above experimental data on the carrier kinetics, it can be assumed that the molecular fluorophores become photobleached under UV irradiation to form new molecular species on the surface of CDs, which can extract excited electrons from the unbleached molecular fluorophores, trap the electrons, and prevent the carrier recombination, leading to the first fast photobleaching decay followed by a prolonged photobleaching decay. On the basis of the above analysis, we propose that the absorption center at 460 nm is attributed to molecular fluorophores, while the absorption center at 512 nm is due to to surface states of the CDs. Considering the deoxidized CD surface after UV irradiation as demonstrated by the XPS results, the decreased surface state absorption and emission should be related to the decreased oxygen content. It can be concluded that UV light-induced deoxidized surface and photobleached molecular fluorophores are beneficial for the enhancement of the intrinsic emission from the carbongenic core of CDs.

A plausible summary of the processes taking place in the CDs and CDs-i is given in Figure 5. The synthesized CDs are presented as a carbonized core (CC) with an oxidized surface with several attached molecular fluorophores (MF), wherein each of these structural elements is an emission center, as shown in the related energy structure scheme. In such CDs, the optical transitions related to MF and surface states possess higher energy than states related to CC. As a result of UV irradiation, MF are almost deteriorated and the CD surface is deoxidized, which leads to a change in the processes of creation and recombination of charge carriers in the CDs. Thus, the number of energy levels related to MF and surface states decreases, which is reflected in a decrease of the optical density and the PL intensity of these bands. As for the optical transitions related to the intrinsic core states, a relative increase in the optical density and in the PL intensity is observed. The accompanied increase of PLQY (from 13% to 17%) together with the prolonged PL lifetime indicate a decrease in the nonradiative relaxation channels (dashed lines in energy scheme, Figure 5 lower panel) upon the UV irradiation.[37,38] Another possible process resulting in the PL enhancement is the decrease of the thermally activated reverse transitions from the intrinsic core emissive state to the closely spaced states with higher energy (shown in Figure 5 as gray dotted lines), because the UV irradiation also induced the deterioration of these energy bands.

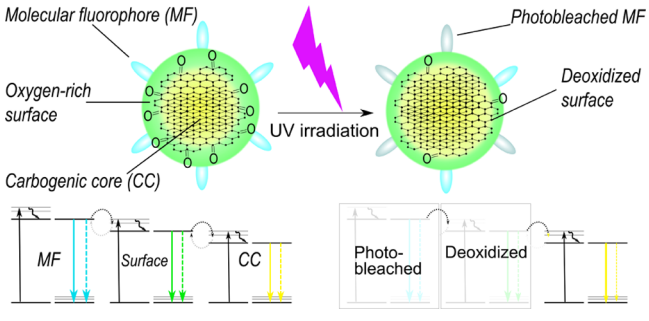

Figure 5. Schematic presentation of (upper panel) a possible structural change from CDs to CDs-i via the UV light-induced deoxidization and photobleaching processes and (lower panel) proposed photophysical processes taking place in CDs (left) and CDs-i (right): internal conversion (black curvy lines), thermally activated transitions (gray dotted lines), absorption (black straight lines), photoluminescence (solid lines), and nonradiative transitions (dashed lines) from molecular fluorophores (MF), cyan lines; surface, green lines; and carbogenic core (CC), yellow lines.

In summary, CDs with three luminescent centers (484, 528, and 550 nm) were synthesized by a microwave-assisted method using phloroglucinol as precursor. It is demonstrated that the observed excitation-dependent luminescence of these CDs is due to varied contributions from the molecular fluorophores, CD surface states, and the intrinsic core CD state into the overall emission signal, while their individual emission bands are excitation-independent. The emission from the surface molecular fluorophores (centered at 484 nm) and the CD surface states (centered at 528 nm) are not photostable and can be photobleached and deoxidized, respectively, after long time UV laser irradiation. In contrast, the emission from the intrinsic state of the inner carbogenic core (centered at 550 nm) exhibits a stable emission with a narrow fwhm of 38 nm. The energy loss caused by the nonradiative relaxation channels together with the thermally activated transitions from the intrinsic state to surface states is eliminated by the UV-irradiation, leading to the enhancement of PL quantum yield from 13% to 17%, which is a realization of relatively pure intrinsic emission. The results of this work provide a new way to improve the intrinsic emission from CDs and are valuable for deeper understanding and controlling the CDs' luminescence origin to promote the development of their application in various fields.

■ ASSOCIATED CONTENT

Supporting Information

The Supporting Information is available free of charge on the ACS Publications website at DOI: 10.1021/acs.jpclett.9b00842.

Experimental Section, Figures S1−S6, and Table S1 (PDF)

■ AUTHOR INFORMATION

Corresponding Author

*E-mail: songnanqu@um.edu.mo.

ORCID

Elena V. Ushakova: 0000-0001-6841-6975

Songnan Qu: 0000-0003-4159-096X

Andrey L. Rogach: 0000-0002-8263-8141

DOI: 10.1021/acs.jpclett.9b00842
J. Phys. Chem. Lett. 2019, 10, 3094−3100

Author Contributions

[⊥]M.S., C.L., Z.T., and E.V.U. contributed equally to this work.

Notes

The authors declare no competing financial interest.

■ ACKNOWLEDGMENTS

This work has been supported by the National Natural Science Foundation of China (Projects 51602304 and 61675049), Youth Innovation Promotion Association of CAS, Jilin Province Science and Technology Research (Projects 20180101190JC, 20170101191JC, 20170101042JC, and 20160520008JH), the Open Project Program of the State Key Laboratory of Supramolecular Structure and Materials in Jilin University (No. sklssm2019014), and the Ministry of Education and Science of the Russian Federation (Grant 14. Y26.31.0028).

■ REFERENCES

(1) Bao, X.; Yuan, Y.; Chen, J.; Zhang, B.; Li, D.; Zhou, D.; Jing, P.; Xu, G.; Wang, Y.; Holá, K.; et al. In Vivo Theranostics with Near-Infrared-Emitting Carbon Dots-Highly Efficient Photothermal Therapy Based on Passive Targeting after Intravenous Administration. *Light: Sci. Appl.* **2018**, *7*, 91.

(2) Qu, D.; Zheng, M.; Li, J.; Xie, Z.; Sun, Z. Tailoring Color Emissions from N-Doped Graphene Quantum Dots for Bioimaging Applications. *Light: Sci. Appl.* **2015**, *4*, No. e364.

(3) Li, D.; Han, D.; Qu, S.-N.; Liu, L.; Jing, P.-T.; Zhou, D.; Ji, W.-Y.; Wang, X.-Y.; Zhang, T.-F.; Shen, D.-Z. Supra-(Carbon Nanodots) with a Strong Visible to Near-Infrared Absorption Band and Efficient Photothermal Conversion. *Light: Sci. Appl.* **2016**, *5*, No. e16120.

(4) Lu, S.; Sui, L.; Liu, J.; Zhu, S.; Chen, A.; Jin, M.; Yang, B. Near-Infrared Photoluminescent Polymer-Carbon Nanodots with Two-Photon Fluorescence. *Adv. Mater.* **2017**, *29*, 1603443.

(5) Jiang, K.; Sun, S.; Zhang, L.; Lu, Y.; Wu, A.; Cai, C.; Lin, H. Red, Green, and Blue Luminescence by Carbon Dots: Full-Color Emission Tuning and Multicolor Cellular Imaging. *Angew. Chem., Int. Ed.* **2015**, *54*, 5360−5363.

(6) Gao, T.; Wang, X.; Yang, L.-Y.; He, H.; Ba, X.-X.; Zhao, J.; Jiang, F.-L.; Liu, Y. Red, Yellow, and Blue Luminescence by Graphene Quantum Dots: Syntheses, Mechanism, and Cellular Imaging. *ACS Appl. Mater. Interfaces* **2017**, *9*, 24846−24856.

(7) Kwon, W.; Do, S.; Kim, J.-H.; Seok Jeong, M.; Rhee, S.-W. Control of Photoluminescence of Carbon Nanodots via Surface Functionalization using Para-substituted Anilines. *Sci. Rep.* **2015**, *5*, 12604.

(8) Yuan, F.; Wang, Z.; Li, X.; Li, Y.; Tan, Z.; Fan, L.; Yang, S. Bright Multicolor Bandgap Fluorescent Carbon Quantum Dots for Electroluminescent Light-Emitting Diodes. *Adv. Mater.* **2017**, *29*, 1604436.

(9) Feng, T.; Zeng, Q.; Lu, S.; Yan, X.; Liu, J.; Tao, S.; Yang, M.; Yang, B. Color-Tunable Carbon Dots Possessing Solid-State Emission for Full-Color Light-Emitting Diodes Applications. *ACS Photonics* **2018**, *5*, 502−510.

(10) Wang, H.; Gao, P.; Wang, Y.; Guo, J.; Zhang, K.-Q.; Du, D.; Dai, X.; Zou, G. Fluorescently Tuned Nitrogen-Doped Carbon Dots from Carbon Source with Different Content of Carboxyl Groups. *APL Mater.* **2015**, *3*, 086102.

(11) Xu, M.; Xu, S.; Yang, Z.; Shu, M.; He, G.; Huang, D.; Zhang, L.; Li, L.; Cui, D.; Zhang, Y. Hydrophilic and Blue Fluorescent N-Doped Carbon Dots from Tartaric Acid and Various Alkylol Amines under Microwave Irradiation. *Nanoscale* **2015**, *7*, 15915−15923.

(12) Ding, H.; Yu, S.-B.; Wei, J.-S.; Xiong, H.-M. Full-Color Light-Emitting Carbon Dots with a Surface-State-Controlled Luminescence Mechanism. *ACS Nano* **2016**, *10*, 484−491.

(13) Holá, K.; Sudolská, M.; Kalytchuk, S.; Nachtigallová, D.; Rogach, A. L.; Otyepka, M.; Zbořil, R. Graphitic Nitrogen Triggers Red Fluorescence in Carbon Dots. *ACS Nano* **2017**, *11*, 12402−12410.

(14) Tian, Z.; Zhang, X.; Li, D.; Zhou, D.; Jing, P.; Shen, D.; Qu, S.; Zboril, R.; Rogach, A. L. Full-Color Inorganic Carbon Dot Phosphors for White-Light-Emitting Diodes. *Adv. Opt. Mater.* **2017**, *5*, 1700416.

(15) Miao, X.; Qu, D.; Yang, D.; Nie, B.; Zhao, Y.; Fan, H.; Sun, Z. Synthesis of Carbon Dots with Multiple Color Emission by Controlled Graphitization and Surface Functionalization. *Adv. Mater.* **2018**, *30*, 1704740.

(16) Vallan, L.; Urriolabeitia, E. P.; Ruipérez, F.; Matxain, J. M.; Canton-Vitoria, R.; Tagmatarchis, N.; Benito, A. M.; Maser, W. K. Supramolecular-Enhanced Charge Transfer within Entangled Polyamide Chains as the Origin of the Universal Blue Fluorescence of Polymer Carbon Dots. *J. Am. Chem. Soc.* **2018**, *140*, 12862−12869.

(17) Ehrat, F.; Bhattacharyya, S.; Schneider, J.; Löf, A.; Wyrwich, R.; Rogach, A. L.; Stolarczyk, J. K.; Urban, A. S.; Feldmann, J. Tracking the Source of Carbon Dot Photoluminescence: Aromatic Domains versus Molecular Fluorophores. *Nano Lett.* **2017**, *17*, 7710−7716.

(18) Ding, H.; Wei, J.-S.; Zhang, P.; Zhou, Z.-Y.; Gao, Q.-Y.; Xiong, H.-M. Solvent-Controlled Synthesis of Highly Luminescent Carbon Dots with a Wide Color Gamut and Narrowed Emission Peak Widths. *Small* **2018**, *14*, 1800612.

(19) Kozák, O.; Sudolská, M.; Pramanik, G.; Cígler, P.; Otyepka, M.; Zbořil, R. Photoluminescent Carbon Nanostructures. *Chem. Mater.* **2016**, *28*, 4085−4128.

(20) Krysmann, M. J.; Kelarakis, A.; Dallas, P.; Giannelis, E. P. Formation Mechanism of Carbogenic Nanoparticles with Dual Photoluminescence Emission. *J. Am. Chem. Soc.* **2012**, *134*, 747−750.

(21) Xiong, Y.; Schneider, J.; Ushakova, E. V.; Rogach, A. L. Influence of Molecular Fluorophores on the Research Field of Chemically Synthesized Carbon Dots. *Nano Today* **2018**, *23*, 124−139.

(22) Yuan, F.; Li, S.; Fan, Z.; Meng, X.; Fan, L.; Yang, S. Shining Carbon Dots: Synthesis and Biomedical and Optoelectronic Applications. *Nano Today* **2016**, *11*, 565−586.

(23) Qu, S.; Shen, D.; Liu, X.; Jing, P.; Zhang, L.; Ji, W.; Zhao, H.; Fan, X.; Zhang, H. Highly Luminescent Carbon-Nanoparticle-Based Materials: Factors Influencing Photoluminescence Quantum Yield. *Part. Part. Syst. Char.* **2014**, *31*, 1175−1182.

(24) Xiong, Y.; Schneider, J.; Reckmeier, C. J.; Huang, H.; Kasák, P.; Rogach, A. L. Carbonization Conditions Influence the Emission Characteristics and the Stability Against Photobleaching of Nitrogen Doped Carbon Dots. *Nanoscale* **2017**, *9*, 11730−11738.

(25) Zhu, S.; Tang, S.; Zhang, J.; Yang, B. Control the Size and Surface Chemistry of Graphene for the Rising Fluorescent Materials. *Chem. Commun.* **2012**, *48*, 4527−4539.

(26) Zhu, S.; Meng, Q.; Wang, L.; Zhang, J.; Song, Y.; Jin, H.; Zhang, K.; Sun, H.; Wang, H.; Yang, B. Highly Photoluminescent Carbon Dots for Multicolor Patterning, Sensors, and Bioimaging. *Angew. Chem., Int. Ed.* **2013**, *52*, 3953−3957.

(27) Qian, Z.; Ma, J.; Shan, X.; Feng, H.; Shao, L.; Chen, J. Highly Luminescent N-Doped Carbon Quantum Dots as an Effective Multifunctional Fluorescence Sensing Platform. *Chem. - Eur. J.* **2014**, *20*, 2254−2263.

(28) Zhu, S.; Zhang, J.; Qiao, C.; Tang, S.; Li, Y.; Yuan, W.; Li, B.; Tian, L.; Liu, F.; Hu, R.; et al. Strongly Green-Photoluminescent Graphene Quantum Dots for Bioimaging Applications. *Chem. Commun.* **2011**, *47*, 6858−6860.

(29) Yuan, F.; Yuan, T.; Sui, L.; Wang, Z.; Xi, Z.; Li, Y.; Li, X.; Fan, L.; Tan, Z.; Chen, A.; et al. Engineering Triangular Carbon Quantum Dots with Unprecedented Narrow Bandwidth Emission for Multicolored LEDs. *Nat. Commun.* **2018**, *9*, 2249.

(30) Lee, D. W.; Seo, J. W. Formation of Phenol Groups in Hydrated Graphite Oxide. *J. Phys. Chem. C* **2011**, *115*, 12483−12486.

(31) Yeh, T.-F.; Chan, F.-F.; Hsieh, C.-T.; Teng, H. Graphite Oxide with Different Oxygenated Levels for Hydrogen and Oxygen Production from Water under Illumination: The Band Positions of Graphite Oxide. *J. Phys. Chem. C* **2011**, *115*, 22587−22597.

(32) Morimoto, N.; Kubo, T.; Nishina, Y. Tailoring the Oxygen Content of Graphite and Reduced Graphene Oxide for Specific Applications. *Sci. Rep.* **2016**, *6*, 21715.

DOI: 10.1021/acs.jpclett.9b00842
J. Phys. Chem. Lett. 2019, 10, 3094−3100

(33) Li, Z. Q.; Lu, C. J.; Xia, Z. P.; Zhou, Y.; Luo, Z. X-Ray Diffraction Patterns of Graphite and Turbostratic Carbon. *Carbon* **2007**, *45*, 1686−1695.
(34) Schindewolf, U. Formation and Properties of Solvated Electrons. *Angew. Chem., Int. Ed. Engl.* **1968**, *7*, 190−203.
(35) Cao, S.; Chen, C.; Liu, T.; Tsang, Y.; Zhang, X.; Yu, W.; Chen, W. Synthesis of Reduced Graphene Oxide/α-$Bi_2Mo_3O_{12}$ @ β-Bi_2O_3 Heterojunctions by Organic Electrolytes Assisted UV-Excited Method. *Chem. Eng. J.* **2014**, *257*, 309−316.
(36) Wang, S.; Wu, Z.-S.; Zheng, S.; Zhou, F.; Sun, C.; Cheng, H.-M.; Bao, X. Scalable Fabrication of Photochemically Reduced Graphene-Based Monolithic Micro-Supercapacitors with Superior Energy and Power Densities. *ACS Nano* **2017**, *11*, 4283−4291.
(37) Wang, Z.; Luo, Z.; Zhao, C.; Guo, Q.; Wang, Y.; Wang, F.; Bian, X.; Alsaedi, A.; Hayat, T.; Tan, Z. Efficient and Stable Pure Green All-Inorganic Perovskite CsPbBr3 Light-Emitting Diodes with a Solution-Processed NiOx Interlayer. *J. Phys. Chem. C* **2017**, *121*, 28132−28138.
(38) Wang, Z.; Wang, F.; Sun, W.; Ni, R.; Hu, S.; Liu, J.; Zhang, B.; Alsaed, A.; Hayat, T.; Tan, Z. Manipulating the Trade-off Between Quantum Yield and Electrical Conductivity for High-Brightness Quasi-2D Perovskite Light-Emitting Diodes. *Adv. Funct. Mater.* **2018**, *28*, 1804187.

DOI: 10.1021/acs.jpclett.9b00842
J. Phys. Chem. Lett. 2019, 10, 3094−3100